IEEE Open Journal of Engineering in Medicine and Biology

Science

EEG microstate as a marker of adolescent idiopathic scoliosis

M. Rubega[1], E. Passarotto[1], M. Paramento[1,2], E. Formaggio[1*] and S. Masiero[1]

[1] Department of Neuroscience, University of Padova, Section of Rehabilitation, Padova, Italy

[2] Department of Information Engineering, University of Padova, Padova, Italy

CORRESPONDING AUTHOR: E. Formaggio (e-mail: emanuela.formaggio@unipd.it)

This work was supported by Fondo di Beneficienza Intesa San Paolo under Grant B/2022/0205, and by REACT EU—PON "Ricerca e Innovazione" 2014–2020, DM 1062/2021

This article has supplementary downloadable material

ABSTRACT —The pathophysiology of Adolescent Idiopathic Scoliosis (AIS) is not yet fully understood, but multifactorial hypotheses have been proposed that include defective central nervous system (CNS) control of posture, biomechanics, and body schema alterations. To deepen CNS control of posture in AIS, electroencephalographic (EEG) activity during a simple balance task in adolescents with and without AIS was parsed into EEG microstates. Microstates are quasi-stable spatial distributions of the electric potential of the brain that last tens of milliseconds. The spatial distribution of the EEG characterised by the orientation from left-frontal to right-posterior remains stable for a greater amount of time in AIS compared to controls. This spatial distribution of EEG, commonly named in the literature as class B, has been found to be correlated with the visual resting state network. Both vision and proprioception networks provide critical information in mapping the extrapersonal environment. This neurophysiological marker probably unveils an alteration in the postural control mechanism in AIS, suggesting a higher information processing load due to the increased postural demands caused by scoliosis.

INDEX TERMS Adolescent Idiopathic scoliosis, Balance, Microstates, Proprioception, Spine.

IMPACT STATEMENT Analysis of the spatial distribution of brain electric potential during a simple standing task in adolescents with AIS revealed a stable and dominant topography, suggesting a higher information processing load.

I. INTRODUCTION

ADOLESCENT Idiopathic Scoliosis (AIS) is a three-dimensional morphological spinal deformity, characterized by the deviation of the spine in the frontal plane (>10 Cobb degrees), the concurrent rotation of the affected vertebral bodies, and most of the time, by the reduction of the physiological curves of the rachis in the sagittal plane [1]. Epidemiological studies report an estimated prevalence of 1-3% among adolescents (10-16 years), with girls being more severely affected [2].

The cause and pathophysiology of AIS is not yet fully understood, but multifactorial hypotheses have been proposed: genetic predisposition, hormonal dysfunction [3] and defective postural control by the central nervous system (CNS) [4]. There is growing evidence of cortical involvement suggesting that AIS could be the expression of a subclinical nervous system disorder. Visuospatial perceptual impairments, alterations in spatial orientation of the body, and sensory integration disorders have been described [5]. According to the neurodevelopmental theories of AIS, a temporal imbalance between musculoskeletal maturation and central sensorimotor integration processes that occur in the posterior parietal cortex would, in turn, result in an improper response of the trunk muscles to compensate for the initiating process of scoliosis [5], [8].

Brain imaging studies suggest that anomalous sensorimotor integration contributes to the cause of AIS, but there is uncertainty about the level of the CNS that causes this dysfunction. An important next step in moving this field forward is to study strategies to reveal the pathogenic mechanism underlying scoliosis. Neuroimaging studies revealed asymmetries in brain stem corticospinal bundles [6], volumetric differences in brain regions functionally related to motor control and coordination [7], abnormal patterns in the motor network during movement execution [8].

Electroencephalography (EEG) allows us to study the electrophysiology of the brain with a millisecond temporal resolution using small, painless sensors attached to the scalp. The first EEG study to report a highly significant difference in the occurrence of paroxysmal EEG activity in AIS compared to controls dates back to the 1970s [9]. An increase in the amplitude of the peak in the alpha rhythm ([7.5-12.5] Hz) was found in the central, frontal, parietal and occipital regions indicating the need for increased cortical processing to maintain balance control in normal upright standing in adolescents with AIS compared to healthy controls [10]. The increase in theta frequency power and suppression of alpha, beta and gamma powers was also observed when proprioception was

altered [11]. Adolescents with AIS were significantly more likely to fail complex sensory-challenged balance tasks when the somatosensory system was stressed by an unstable position of the feet, particularly when the eyes were closed [12].

To simultaneously consider signals recorded in all areas of the cortex and assess whether there is a disruption of the large brain network associated with AIS, we applied the *microstates* analysis in a previous published dataset [13]. Microstate analysis is a data-driven approach considering multichannel EEG recording as a series of quasi-stable spatial distributions that are each characterized by a unique topography of electric potentials over the entire channel array [14]. These unique topographies last for tens of milliseconds and then abruptly change in the following one. These different topographical patterns termed microstates (MS) directly indicate changes in the configuration of neuronal generators that represent elementary short-lasting periods of coordinated synchronized communication within large-scale brain networks [15]. Four standard microstates, labeled A, B, C, and D, have been shown to be consistent throughout age and account for 79% of the variance on the average of the input EEG data of 496 subjects [18]. These four standard microstates have been identified both at rest and during task performance [24]. Based on the temporal sequence of the four standard microstate maps, brain activity in wakefulness is described in terms of the duration, the rate of occurrence, and the transition sequences of each map [19]. A lot of studies reported that microstate parameters are affected by pathology, visual, and verbal tasks [26].

Most studies selected the four microstates based on the existing literature [14]. Although the topographies of these four microstates are fairly stable across studies, examples of atypical maps are found in which classification into canonical A-B-C-D classes and subsequent functional interpretations may be too restrictive [17]. For this reason, in [17], the authors estimated seven topographies of resting-state explaining 84% of the global variance of the EEG data of 164 subjects with k-means clustering.

In this work, we used a k-mean clustering method to estimate the optimal set of microstates explaining the input EEG signal from three groups (14 girls with AIS - 10 with a right curve and 4 with a left curve - and 14 girls without AIS). Clustering EEG data at Global Field Power (GFP) peaks to maximize the signal-to-noise ratio and focus on moments of high global neuronal synchronization [17], [18], [20] led to six microstates that explained more than 80% of the global variance of the input EEG signal. Then each time point of the original EEG signal was exclusively assigned to one of these six microstates. Duration (s in which the same microstate is assigned to consecutively time points), Occurence (how many times the same microstate appears every s) and Total Time Coverage (the percentage of time points assigned to the same microstates during the whole recording) let us identify one microstate characterizing the dynamics of the overall brain activity of girls with AIS during the experimental task.

By analysing the topography recorded by multichannel electrode arrays, rather than analysing the activity recorded by each electrode independently, we aim to identify changes in the global network of brain activity in AIS, particularly during posture. The temporal sequence of microstates provides an ideal macroscopic window to observe the temporal dynamics of overall brain activity. Changes in topography indicate changes in the global coordination of neuronal activity over time [24].

II. RESULTS

A. Participants

Fourteen adolescent girls with a confirmed diagnosis of AIS (10 with right (right AIS) main curve and 4 with left (left AIS) main curve) and fourteen adolescent girls without AIS (age-matched controls (CTRL)) stood upright with eyes closed and with their arms raised laterally to 90° for 1 min (Fig. 1a). With this task, we expect only in adolescents with AIS an asymmetrical activation of the sensorimotor brain areas [13] to counteract the effect of the scoliotic curve (i.e, an asymmetrical activation of the spinal muscles). EEG signals (32-channels system; BrainAmp 32MRplus, BrainProducts GmbH, Munich, Germany) were acquired using an analog anti-aliasing band pass-filter at 0.1–1000 Hz and converted from analog to digital using a sampling rate of 500 Hz. The reference was between Fz/Cz and ground anterior to Fz (Fig. 1b).

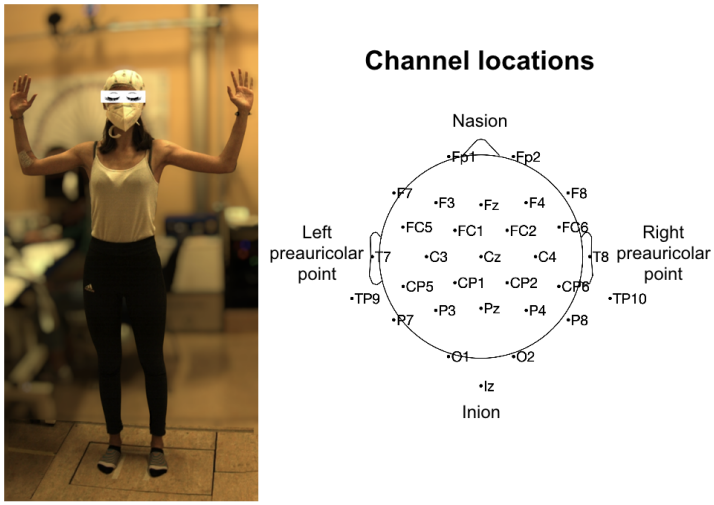

Fig. 1: The left panel depicts a participant standing upright with eyes closed and with arms raised laterally to 90° whilst wearing the EEG cap. The right panel displays the channel locations according to the 10-10 system.

For further details on the database, we refer the reader to [13].

B. Grand Grand Mean Template

By investigating the EEG electric potential amplitude of all channels as a topographic voltage map at each time point, we segmented the EEG data, seen as a topographic flow, into a series of meta-stable topographic configurations, each lasting several tens of milliseconds. We chose to exploit 6 maps (Fig. 2, upper panel). Six maps explained most of the data (Fig. 5, upper panel): 80% on average for the right AIS; 81% for the left AIS and 84% for CTRL.

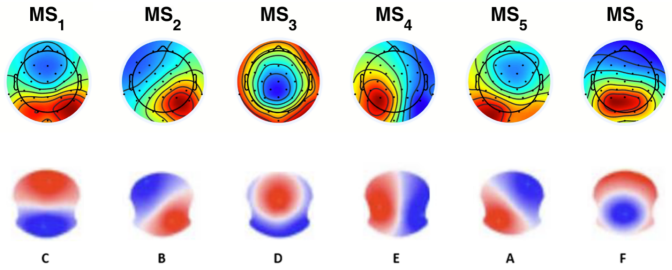

Fig. 2: Microstates maps (MS). The first row report MS computed from the data analyzed in this work. The second row report MS from [17].

Get that there is not yet a gold-standard to choose the appropriate number of maps, the main criteria adopted in this work was: (i) the consistency of the maps between the three groups [23]; (ii) the assignment of all maps to previously identified microstate types [17]; (iii) the average amount of variance explained in the data being at least 80%. Taking as reference [17] (Fig. 2, lower panel) and ignoring polarity, the microstates depicted in the first row of Fig. 2, might be labeled – from left to right – as C, B, D, E, A and F. We found among these 6 maps the four standard microstates (MS_5 as map A, MS_2 as map B, MS_1 as map C, MS_3 as map D).

C. Microstates duration

We quantified how many seconds each microstate lasts in the topographical flow of each subject (Fig. 3). The duration of MS_2 characterized girls with right AIS. Indeed – as reported in Fig. 3 – MS_2 lasted a greater amount of ms in right AIS (*median* = 65 ms, [56, 74] ms) compared to CTRL (*median* = 59 ms, [49, 70] ms) and, on average, was the MS with the longest duration in right AIS. These observations were confirmed by Bayesian mixed effects regression models (see the Statistical analysis section and Table I). We identified a significant MS:group interaction when comparing MS_2 duration values between right AIS and CTRL, $\beta = 0.100$ [0.008, 0.191]. This difference did not generalize to patients with left AIS, who showed duration values comparable to controls. The analyses of TTC and occurrence values did not lead to any meaningful findings.

III. DISCUSSION

This study reports for the first time microstates EEG results derived from AIS subjects. Our results revealed a stable and dominant topography (map B) in adolescents with right AIS standing upright with eyes closed and arms raised. Map B (MS_2) lasts the greatest amount of time (i.e., MS_2 has the longest duration) compared to all the other maps of AIS and controls. In [20], microstate map B matched with fMRI resting state networks previously attributed to visual imagery. In [27], a strong generator in the posterior brain cortex and an additional generator in right occipital brain areas was supposed to produce microstate map B. Secondary visual processing was associated with the right-posterior parietal cortex [28]. Using fMRI data during tactile discrimination tasks, under ambient light and

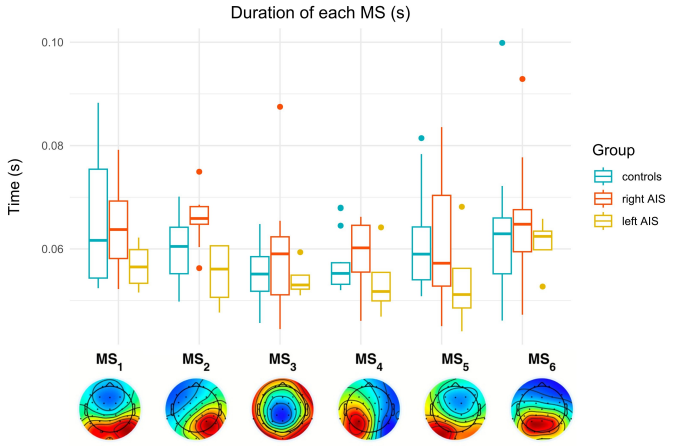

Fig. 3: Duration of microstates maps. On each box, the central line indicates the median, and the bottom and top edge of the box indicate the 25th and 75th percentiles, respectively. The whiskers extend to the most extreme data points not considered outliers, and the outliers are plotted individually using the • symbol. Blue boxes refer to durations for CTRL, orange ones for right AIS and yellow ones for left AIS. Y-axis reports durations in s and X-axis the six microstates maps.

Fixed effects	Estimate	Est.Error	lower CI	upper CI
MS1	-2.728	0.045	-2.816	-2.640
MS2	-2.821	0.03	-2.882	-2.762
MS3	-2.894	0.039	-2.970	-2.816
MS4	-2.865	0.033	-2.930	-2.802
MS5	-2.798	0.046	-2.892	-2.708
MS6	-2.766	0.049	-2.863	-2.669
MS1:right_AIS	-0.023	0.070	-0.159	0.118
MS2:right_AIS	0.100	0.046	0.008	0.191
MS3:right_AIS	0.053	0.060	-0.067	0.172
MS4:right_AIS	0.038	0.051	-0.061	0.139
MS5:right_AIS	-0.011	0.072	-0.155	0.128
MS6:right_AIS	0.026	0.078	-0.131	0.184
MS1:left_AIS	-0.144	0.094	-0.328	0.038
MS2:left_AIS	-0.077	0.063	-0.198	0.054
MS3:left_AIS	-0.023	0.083	-0.181	0.138
MS4:left_AIS	-0.061	0.069	-0.194	0.079
MS5:left_AIS	-0.136	0.098	-0.325	0.064
MS6:left_AIS	-0.035	0.106	-0.247	0.164

TABLE I: Bayesian mixed effects model. The table reports the estimates and 95% credible intervals of the fixed effects.

in complete darkness, Brodoeh et al. demonstrated that eye closure improved somatosensory perception not merely due to the lack of visual signals. The act of closing the eyes itself altered the processing mode in the brain, i.e., eye closure significantly increased occipital blood-oxygen-level-dependent activity in the areas of somatosensory and secondary visual processing [29].

Postural control depends on proper integration of proprioceptive, visual, and vestibular information at the central level [16]. Human balance during an upright stance is more unstable with eyes closed than with eyes open, proving the importance

of the visual network. Some studies [10], [11] have reported similar balance control between AIS and controls, and thus no indication of deficient balance in AIS, when the somatosensory system was stable (i.e., during upright static stance with eyes open or closed). This finding changes when the balance control task is challenged (e.g., by an unstable position of the feet or with arms up, particularly when the eyes are closed). Removing visual information when standing upright with arms raised would exacerbate balance control of AIS participants more than the one of control participants, and this can be reflected by the longer duration of map B.

We argue that girls with AIS need longer activation of somatosensory and secondary visual processing areas than CTRL during a static balance task with eyes closed. This longer duration of map B probably represents the higher information processing load in girls with AIS. This finding supports our previous results. We found in the same dataset an increase in theta activity and alpha lateralization in girls with AIS. We assumed that it may be a compensatory strategy to overcome sensorimotor dysfunction mirrored by altered body schema [13]. Moreover, a diffusion tensor imaging analysis found a reduction of fractional anisotropy in fibers interconnecting the primary somatosensory cortex and visual cortex in patients with AIS [33]. Xue et al. suggested that the above microstructural changes might be related to the somatosensory function impairment and visuo-oculomotor dysfunction in AIS [33].

IV. CONCLUSION

Our study does not claim to distinguish between the cause and the effect of scoliosis, but it does support research into the involvement of the CNS in this condition. Indeed, the spatial distribution of electrical potential during a simple standing task in adolescents with AIS showed a stable and dominant topography, suggesting a higher information processing load due to increased postural demands in girls with scoliosis. Duration of map B could be a valuable marker of information processing in AIS. Future studies could monitor the duration of map B in the long term, and investigate a possible correlation between this electrophysiological marker and the progression of scoliosis.

V. MATERIALS AND METHODS

A. Ethics clearance

Ethical approval has been obtained from the Ethics Committee of the University Hospital of Padova (n. 5627/AO/22 AOP 2836) on 13 April 2023.

B. Microstate analysis

Topographic EEG analysis was performed using the previously described microstate approach [25] and the EEGLAB tool designed by Koenig [21]. This analysis is based on a two-stage process to obtain the prototype topographies, which best explain the signal variance. The computation of EEG microstate topographies is performed conventionally on EEG data band-pass filtered from 2 to 20 Hz [18]. EEG data were band-pass filtered in [2-20] Hz by a windowed-sinc filter (Hamming window) avoiding phase distortion.

First, for each subject, the time points of the maximum Global Field Power (GFP), i.e.,

$$\mathrm{GFP_c(t)} = \sqrt{\frac{\sum_{\mathrm{i}=1}^{\mathrm{N}} (\mathrm{c_i(t)} - \bar{\mathrm{c}}(\mathrm{t}))^2}{\mathrm{N}}} \tag{1}$$

where $c_i(t)$ is the voltage potential at electrode i and $\bar{c}(t)$ is the average voltage potential of all electrodes at the time point t and $N = 30$ is the number of electrodes, were selected as the moments of high global neuronal synchronization. For each subject, the topographies of these time points were then clustered independently using a k-means clustering approach. This step was repeated for a number of clusters from 3 to 8.

In a second step, the optimal clusters of each subject were again clustered together to find the common template maps for each of the three groups and the average topographical map was then calculated for each cluster (obtaining the microstates maps for each group, i.e., the *grand mean template*). We used the "elbow" or "knee of a curve" to select the number of clusters. This is a common heuristic in mathematical optimization to choose the number of clusters so that adding another cluster does not provide much better modeling of the data. The lower panel of Fig. 5 shows the elbow graph that represents on the y-axis the differences in explained variance as function of k (i.e., number of maps). For instance, the values corresponding to the number of MS equal to 4 in the lower panel of Fig. 5 represents the difference between the explained variance exploiting $k = 4$ MS and the explained variance exploiting $k = 3$ MS. We picked the k-value where the elbow was created.

This step was repeated to obtain the common template maps for all subjects (considering all three groups), i.e., the *grand grand mean template*.

Finally, these common templates were fitted back to the original EEG, and each time point t was competitively labeled with the cluster maps based on the Global Map Dissimilarity (GMD) measure.

$$\mathrm{GMD}(t) = \sqrt{\frac{1}{N}\sum_{i=1}^{N}\left(\frac{c_i(t)-\bar{c}(t)}{GFP_c(t)} - \frac{v_i(t)-\bar{v}(t)}{GFP_v(t)}\right)^2} \tag{2}$$

where $c_i(t)$ is the voltage potential at electrode i and $\bar{c}(t)$ is the average voltage potential of all electrodes at time t in the map c while $v_i(t)$ is the voltage potential at electrode i, $\hat{v}(t)$ is the average voltage potential of all electrodes at time t in the map v and $N = 30$ is the number of electrodes. GMD is equivalent to the spatial Pearson's product-moment correlation coefficient between the potentials of the template map and the instant topography. This resulted in the microstate sequence, as a sequence of the cluster labels (Fig. 4). Extracting six clusters resulted in highly comparable microstate maps among the three groups, seven (or more) clusters yielded inconsistent combinations of microstate maps among the three groups.

To compare the microstates sequences and dynamics among the three groups, the following parameters were computed: 1) the total time coverage (TTC) giving the percent of total time

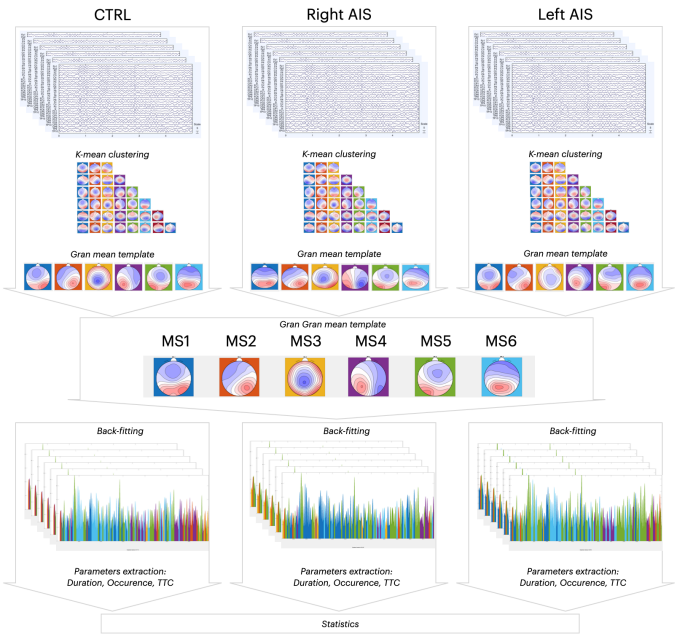

Fig. 4: Steps of microstate analysis. The EEG data recorded in the three groups are seen as a topographic voltage map at each time point. The topographies at each time point are clustered indipendently using a k-means clustering approach. The number of cluster varies from 3 to 8. Then, the optimal cluster of each subject are clustered together to find the common template maps for each group (grand mean template). Then, these maps are clustered togheter to find the common template for all groups (grand grand mean template). The grand grand mean template is fitted back to the original EEG of each subject obtaining a microstate sequence for each subject. From these sequences, it is possible to compute the microstate parameters and then compared them by proper statistics methods.

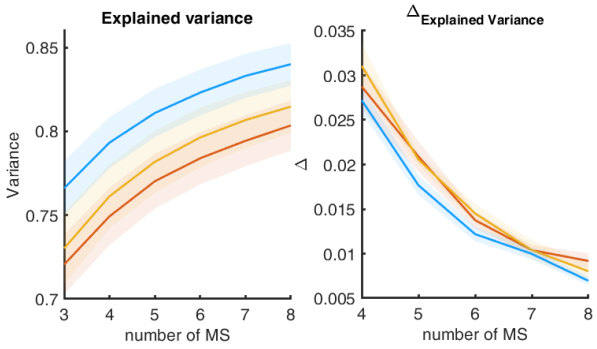

Fig. 5: Data explained variance by microstates maps. The left panel reports the mean (bold line) and the standard deviation (shadowed area) of the data explained variance by the microstates maps reported in the first row of Fig. 2 for each group (blue for controls, red for right AIS, yellow for left AIS). The right panel reports the difference between the values reported in the left panel to highlight that exploiting more than 6 maps would add less than 1% of explained variance on average.

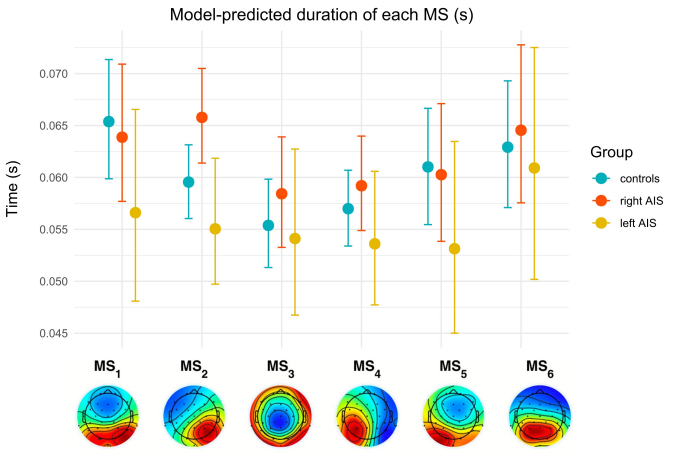

Fig. 6: Model predictions. The duration of microstates maps were estimated from the Bayesian mixed-effects model coefficients reported in Table 1. Dots indicate the effect estimates and microstates map while error bars represent 95% credible intervals of each estimate. Blue error bars refer to durations for CTRL, orange ones for right AIS and yellow ones for left AIS. Y-axis reports durations in s and X-axis the six microstates maps.

in the EEG recording, covered by each microstate class; 2) the duration for each microstate class; and 3) the occurrence, i.e., occurrences/s describing the average number of appearances for the same microstate per second. We did not analysed the transition probabilities since they have been shown to be much less reliable than duration, total time coverage, and occurrence values [22], [23].

C. Statistical analysis

Group-differences in microstates parameters were assessed by Bayesian mixed-effects regression models. TTC, duration, and occurrence were entered as dependent variables and were regressed on MS and group:MS interaction. MS was modelled as a categorical predictor. In addition, the slopes of MS were allowed to vary across subjects, as a random effect. The model intercept was fixed to 0 and the CTRL group was taken as a reference. Duration was modelled via gamma probability distributions and logarithmic link functions.

Therefore, the dependent variable is expressed as:

$$y \sim \mathcal{N}\left(\beta_1(MS) + \beta_2(MS:group) + \gamma_{1,\text{subj}}(MS), \sigma^2\right) \quad (3)$$

and the random effect is modelled as a zero-mean normal distribution:

$$\gamma_{1,\text{subj}} \sim \mathcal{N}\left(\mathbf{0}, \tau^2\right) \quad (4)$$

Only the analyses of duration values lead to the identification of significant group differences and are included in the present manuscript (the input of the Statistic analysis – i.e., TTC, duration, occurrence for each subject and MS – is reported in the Supplementary material as an .xls file). Regression coefficients are here reported on the log-transformed scale, followed by 95% credible intervals (CI) in square brackets.

VI. CONFLICT OF INTEREST

The authors have no conflicts of interest.

VII. AUTHOR CONTRIBUTIONS

Maria Rubega, Emanuela Formaggio and Stefano Masiero designed the project; Stefano Masiero granted financial support; Maria Rubega and Emanuela Formaggio conceived the experiment; Maria Rubega and Emanuela Formaggio recorded the data; Maria Rubega, Edoardo Passarotto, Matilde Paramento analyzed EEG data; Edoardo Passarotto run the statistics; Maria Rubega and Edoardo Passarotto drafted the manuscript; Matilde Paramento, Emanuela Formaggio contributed to manuscript editing; Stefano Masiero reviewed the manuscript. All authors critically discussed the results.

REFERENCES

[1] Negrini, S., Donzelli, S., Aulisa, A. G., Czaprowski, D., Schreiber, S., de Mauroy, J. C., ... and Zaina, F. (2018). 2016 SOSORT guidelines: orthopaedic and rehabilitation treatment of idiopathic scoliosis during growth. Scoliosis and spinal disorders, 13(1), 1-48.

[2] Weinstein, S. L., Dolan, L. A., Cheng, J. C., Danielsson, A., and Morcuende, J. A. (2008). Adolescent idiopathic scoliosis. The lancet, 371(9623), 1527-1537.

[3] Sil Silva, R. T. E., Fernandes, R. J. R., Ono, A. H. D. A., MARCON, R., Cristante, A. F., and BARROS, T. E. P. D. (2017). Role of different hormones in the pathogenesis and severity of adolescent idiopathic scoliosis. Acta ortopedica brasileira, 25, 15-17.

[4] Herman, R., Mixon, J., Fisher, A., Maulucci, R., and Stuyck, J. (1985). Idiopathic scoliosis and the central nervous system: a motor control problem. The Harrington lecture, 1983. Scoliosis Research Society. Spine, 10(1), 1-14.

[5] Burwell, R. G., and Dangerfield, P. H. (2012). Whither the etiopathogenesis (and scoliogeny) of adolescent idiopathic scoliosis. Stud Health Technol Inform, 176, 3-19.

[6] Geissele, A. E., Kransdorf, M. J., Geyer, C. A., Jelinek, J. S., and Van Dam, B. E. (1991). Magnetic resonance imaging of the brain stem in adolescent idiopathic scoliosis. Spine, 16(7), 761-763.

[7] Liu, T., Chu, W. C., Young, G., Li, K., Yeung, B. H., Guo, L., ... and Cheng, J. C. (2008). MR analysis of regional brain volume in adolescent idiopathic scoliosis: neurological manifestation of a systemic disease. Journal of Magnetic Resonance Imaging: An Official Journal of the International Society for Magnetic Resonance in Medicine, 27(4), 732-736.

[8] Domenech, J., García-Martí, G., Martí-Bonmatí, L., Barrios, C., Tormos, J. M., and Pascual-Leone, A. (2011). Abnormal activation of the motor cortical network in idiopathic scoliosis demonstrated by functional MRI. European Spine Journal, 20, 1069-1078

[9] Petersen, I., Sahlstrand, T., and Sellden, U. (1979). Electroencephalographic investigation of patients with adolescent idiopathic scoliosis. Acta Orthopaedica Scandinavica, 50(3), 283-293.

[10] Lanthier, J., Simoneau, M., Knoth, I. S., Lippé, S., Bluteau, C., and Fortin, C. (2020). Increased EEG alpha peak frequency in adolescents with idiopathic scoliosis during balance control in normal upright standing. Neuroscience letters, 722, 134836.

[11] Fortin, C., Pialasse, J. P., Knoth, I. S., Lippé, S., Duclos, C., and Simoneau, M. (2019). Cortical dynamics of sensorimotor information processing associated with balance control in adolescents with and without idiopathic scoliosis. Clinical Neurophysiology, 130(10), 1752-1761.

[12] Byl, N. N., Holland, S., Jurek, A., and Hu, S. S. (1997). Postural imbalance and vibratory sensitivity in patients with idiopathic scoliosis: implications for treatment. Journal of Orthopaedic & Sports Physical Therapy, 26(2), 60-68.

[13] Formaggio, E., Bertuccelli, M., Rubega, M., Di Marco, R., Cantele, F., Gottardello, F., ... and Masiero, S. (2022). Brain oscillatory activity in adolescent idiopathic scoliosis. Scientific Reports, 12(1), 17266.

[14] Khanna, A., Pascual-Leone, A., Michel, C. M., and Farzan, F. (2015). Microstates in resting-state EEG: current status and future directions. Neuroscience & Biobehavioral Reviews, 49, 105-113.

[15] Gschwind, M., Hardmeier, M., Van De Ville, D., Tomescu, M. I., Penner, I. K., Naegelin, Y., ... and Seeck, M. (2016). Fluctuations of spontaneous EEG topographies predict disease state in relapsing-remitting multiple sclerosis. NeuroImage: Clinical, 12, 466-477.

[16] Winter, D.A.(1995). Human balance and posture control during standing and walking. Gait & posture, 3(4), 193-214.

[17] Custo, A., Van De Ville, D., Wells, W. M., Tomescu, M. I., Brunet, D., and Michel, C. M. (2017). Electroencephalographic resting-state networks: source localization of microstates. Brain connectivity, 7(10), 671-682.

[18] Koenig, T., Prichep, L., Lehmann, D., Sosa, P. V., Braeker, E., Kleinlogel, H., ... and John, E. R. (2002). Millisecond by millisecond, year by year: normative EEG microstates and developmental stages. Neuroimage, 16(1), 41-48.

[19] Brodbeck, V., Kuhn, A., von Wegner, F., Morzelewski, A., Tagliazucchi, E., Borisov, S., ... and Laufs, H. (2012). EEG microstates of wakefulness and NREM sleep. Neuroimage, 62(3), 2129-2139

[20] Britz, J., Van De Ville, D., and Michel, C. M. (2010). BOLD correlates of EEG topography reveal rapid resting-state network dynamics. Neuroimage, 52(4), 1162-1170.

[21] Koenig, T. (2017). The EEGLAB plugin for Microstates https://www.thomaskoenig.ch/index.php/work/software/10-eeglab-plugin-manual

[22] Antonova, E., Holding, M., Suen, H. C., Sumich, A., Maex, R., and Nehaniv, C. (2022). EEG microstates: Functional significance and short-term test-retest reliability. Neuroimage: Reports, 2(2), 100089.

[23] Kleinert, T., Koenig, T., Nash, K., and Wascher, E. (2023). On the reliability of the EEG microstate approach. Brain topography, 1-16.

[24] Michel, C. M., and Koenig, T. (2018). EEG microstates as a tool for studying the temporal dynamics of whole-brain neuronal networks: a review. Neuroimage, 180, 577-593.

[25] Brunet, D., Murray, M. M., and Michel, C. M. (2011). Spatiotemporal analysis of multichannel EEG: CARTOOL. Computational intelligence and neuroscience, 2011, 1-15.

[26] Milz, P., Faber, P. L., Lehmann, D., Koenig, T., Kochi, K., and Pascual-Marqui, R. D. (2016). The functional significance of EEG microstates—Associations with modalities of thinking. Neuroimage, 125, 643-656.

[27] Pascual-Marqui, R. D., Lehmann, D., Faber, P., Milz, P., Kochi, K., Yoshimura, M., ... and Kinoshita, T. (2014). The resting microstate networks (RMN): cortical distributions, dynamics, and frequency specific information flow. arXiv preprint arXiv:1411.1949.

[28] Malhotra, P., Coulthard, E. J., and Husain, M. (2009). Role of right posterior parietal cortex in maintaining attention to spatial locations over time. Brain, 132(3), 645-660.

[29] Brodoehl, S., Klingner, C. M., & Witte, O. W. (2015). Eye closure enhances dark night perceptions. Scientific reports, 5(1), 10515.

[30] Adler, N., Bleck, E.E., Rinsky, L.A., Young, W. (1986). Balance reactions and eye-hand coordination in idiopathic scoliosis. J Orthop Res., 4(1), 102-7.

[31] Byl, N.N., Holland, S., Jurek, A., Hu, S.S. (1997). Postural imbalance and vibratory sensitivity in patients with idiopathic scoliosis: implications for treatment. J Orthop Sports Phys Ther, 26(2), 60-8.

[32] Le Berre, M., Guyot, M. A., Agnani, O., Bourdeauducq, I., Versyp, M. C., Donze, C., Thévenon, A., Catanzariti, J. F. (2017). Clinical balance tests, proprioceptive system and adolescent idiopathic scoliosis. European Spine Journal, 26, 1638-1644.

[33] Xue, C., Shi, L., Hui, S. C. N., Wang, D., Lam, T. P., Ip, C. B., ... and Chu, W. C. W. (2018). Altered white matter microstructure in the corpus callosum and its cerebral interhemispheric tracts in adolescent idiopathic scoliosis: diffusion tensor imaging analysis. American Journal of Neuroradiology, 39(6), 1177-1184.